CHEMISTRY
A EUROPEAN JOURNAL

DOI: 10.1002/chem.200600031

Syntheses, Structural Studies, and Magnetic Properties of Divalent Cu and Co Selenites with Organic Constituents

Mei-Ling Feng,[a] Andrey V. Prosvirin,[b] Jiang-Gao Mao,*[a] and Kim R. Dunbar[b]

Abstract: Six new divalent metal selenites have been synthesized by hydro-/solvothermal methods which leads to the incorporation of the organic template as a cation or a ligand. The structure of $[H_2pip][Cu(SeO_3)_2]$ (**1**) (pip = piperazine) features 1D anionic chains of $[Cu(SeO_3)_2]^{2-}$ which are cross-linked by the template cations through hydrogen bonds into a 2D layer. In $[Cu(C_3H_4N_2)(SeO_3)]$ (**2**) the organic template is coordinated to the copper(II) ion of the inorganic $Cu(SeO_3)$ layer. The isostructural compounds $[H_2en][M(HSeO_3)_2Cl_2]$ (en = ethylenediamine; M = Cu (**3**), Co (**4**)) contain layers of $[MCl_2(HSeO_3)_2]^{2-}$ units (M = Cu, Co), which are cross-linked by the template cations via hydrogen bonds into a 3D network. The structure of $[H_2en][Cu_2(SeO_3)_2(HSeO_3)]_2 \cdot H_2O$ (**5**), consists of a pillared layered architecture in which the $Cu(SeO_3)$ layers are further interconnected by bridging hydrogen selenite groups (the pillar). The compound $[H_2pip][Cu_2(Se_2O_5)_3]$ (**6**), which crystallizes as a 3D open framework represents the first organically templated metal diselenite. These new compounds are thermally stable up to at least 170 °C. All of the compounds exhibit fairly strong antiferromagnetic interactions. More interestingly, compounds **3** and **4** behave as a weak ferromagnets below the critical temperatures of $T_c =$ 12 and 8 K, respectively, and both of them exhibit spin-flop phase transitions around 800 ± 100 Oe.

Keywords: hydrothermal synthesis · magnetic properties · open framework · selenites

Introduction

The widespread applications of open-framework inorganic materials in heterogeneous catalysis, separations, and ion-exchange processes have stimulated considerable research interest in the use of organic templates to direct the synthesis of porous materials.[1] Many of these materials are synthesized in the presence of organic amines as structure-directing agents, which usually occupy the structural voids and are well-isolated from the inorganic skeleton.[1] A remarkable variety of such materials have been reported,[2] in particular those based on phosphate ligands,[2,3] but open frameworks of metal arsenates;[4–6] germinates[7,8] and carbonates[9] are also known. Recently, this research field has been extended to the oxo-anions of Group 16 elements. The stereochemically active lone pair electrons of selenium(IV) and tellurium(IV) ions have a dramatic effect on their coordination geometry as well as on the structures of their metal complexes. It has been reported that the asymmetric coordination geometry adopted by selenium(IV) or tellurium(IV) atoms may aid in the crystallization of metal selenites in non-centrosymmetric space groups which is of interest for engendering interesting physical properties such as nonlinear optical second-harmonic generation (SHG).[10] In the case of metal selenites, the first organically templated zinc selenite with a layered structure, $(CN_3H_6)_4[Zn_3(SeO_3)_5]$, was reported recently by Harrison and co-workers.[11] The first three-dimensional organically templated Fe^{III} selenite, $(C_4N_2H_{12})_{0.5}[Fe_2F_3(SeO_3)_2]$, and an organically pillared zinc selenite, $[C_2N_2H_8]_{0.5}(ZnSeO_3)$, were reported by Rao et al., several years ago.[12] Both organically templated and organically linked vanadium selenites have also been synthesized and structurally characterized.[13,14] More recently, examples

[a] Dr. M.-L. Feng, Prof. J.-G. Mao
State Key Laboratory of Structural Chemistry
Fujian Institute of Research on the Structure of Matter
Chinese Academy of Sciences
Fujian, Fuzhou 350002 (PR China)
and
Graduate School of the Chinese Academy of Sciences
Beijing, 100039 (PR China)
Fax: (+86) 591-83714946
E-mail: mjg@ms.fjirsm.ac.cn

[b] Dr. A. V. Prosvirin, Prof. K. R. Dunbar
Department of Chemistry
Texas A&M University
PO Box 30012, College Station, TX 77843-3012 (USA)

Supporting information for this article is available on the WWW under http://www.chemistry.org or from the author.

of organically templated transition metal selenites, $[NH_2(CH_2)_4NH_2]_{0.5}[M(HSeO_3)(Se_2O_5)]$ (M = Zn, Co, Ni), $[H_2N(CH_2)_2NH_2][CdCl_2(HSeO_3)_2]$, $[H_2N(CH_2)_2NH_2]_2[Zn_4(SeO_3)_4]$, and $[H_3N(CH_2)_3NH_3]_4[Zn_4(SeO_3)_8]$ have appeared in the literature.[15–17] Finally a number of organically templated or bonded Mo^{VI} selenites based on polyoxomolybdate cluster units have been isolated, with the SeO_3 group in such compounds acting as a capping group for the Mo^{VI} cluster.[18]

The aforementioned results notwithstanding, the chemistry of metal selenites is still in its infancy and more systematic research studies are needed in order for the full appreciation of this rich area of chemistry to be realized. The aim of the present study is to understand the effects of the experimental conditions, in particular the template used in the synthesis of the copper(II) and cobalt(II) selenites. The copper(II) ion can adopt several types of coordination geometries and selenium(IV) is known to form several different anions such as SeO_3^{2-}, $HSeO_3^-$ and $Se_2O_5^{2-}$ depending on experimental conditions. Hence one can expect that a variety of organically templated copper(II) selenites with novel structures and interesting magnetic properties are possible. Herein we report six new divalent metal selenites by hydro-/solvothermal methods. The compounds crystallize in architectures ranging from 1D chains to 3D networks and exhibit interesting magnetic properties including spin-flop behavior for two of them. The copper(II) compounds represent the first examples of organically templated selenite containing materials with this transition metal.

Results and Discussion

Synthesis

Hydro-/solvothermal synthesis is an effective method for the preparation of organically templated selenites. Compounds **1** and **5** were synthesized by using CuCN as the source of the copper(I) ion and **2** was prepared from CuCl. The copper(I) is oxidized to copper(II) which most likely occurs with reduction of SeO_2 (Se^{4+}/Se 0.74 V). The use of $CuCl_2$ for attempted preparations of **1**, **2** and **5** resulted only in the formation of **3**. The selenium(IV) atom in the products is present as a selenite, hydrogen selenite or diselenite group.

Single crystal X-ray studies

$[H_2pip][Cu(SeO_3)_2]$ (1): Structural determination of compound **1** reveals that it consists of 1D chains of $[Cu(SeO_3)_2]^{2-}$ anions. The asymmetric unit consists of eight non-hydrogen atoms, five of which belong to the inorganic framework (one Cu atom, one Se atom and three O atoms) and three of which belong to the template cation (two C and one N) (Figure 1). The coordination geometry around the copper(II) ion can be described as a slightly distorted square-planar environment with four oxygen atoms being donated from four SeO_3^{2-} groups. The Cu–O distances

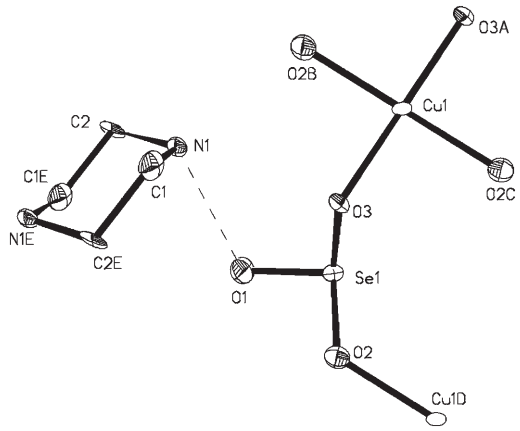

Figure 1. Selected unit of **1**. Thermal ellipsoids are drawn at 50% probability. Symmetry codes for generated atoms: a) $-x+1, -y+1, -z+1$; b) $x-1, y, z$; c) $-x+2, -y+1, -z+1$; d) $x+1, y, z$; e) $-x+1, -y, -z+2$.

range from 1.965(6) Å to 1.982(7) Å. The O-Cu-O bond angles between two *trans* oxygen atoms are 180° whereas those for two *cis* oxygen atoms deviate slightly from the ideal 90° (Table 2). The SeO_3 unit, which acts as a bidentate linker, is tetrahedral with the forth coordination site being occupied by a lone pair. The O1 of the selenite group is not coordinated. Each pair of copper(II) ions are bridged by a pair of selenite groups into a 1D anionic chain of $[Cu(SeO_3)_2]^{2-}$ along the *a* axis (Figure 2a). The H_2pip cation forms hydrogen bonds with two selenite oxygen atoms from different chains by using its two amine groups. The N1–H01b···O1 bond length and angle are 2.70(1) Å and 172.8°, respectively (Table 2). The hydrogen bonding results in a (011) 2D layer motif (Figure 2b).

$Cu(C_3H_4N_2)(SeO_3)$ (2): The use of imidazole as a potential template molecule led to the formation of the copper selenite, $[Cu(C_3H_4N_2)(SeO_3)]$ (**2**), with the organic molecule acting as a ligand. As shown in Figure 3, the asymmetric unit of **2** consists of ten independent non-hydrogen atoms, five of which belong to the inorganic framework (one Cu atom, one Se atom and three O atoms), and five of which are from the imidazole ligand (two N atoms and three C atoms). The Cu ion is five-coordinate, being surrounded by one N atom from an imidazole and four O atoms from independent selenite groups. The coordination geometry around the copper(II) ion is a distorted square pyramid. The Cu1–O12c distance of 2.238(7) Å is significantly longer than the remaining Cu1−O bonds [1.930(7)–2.080(7) Å]. The selenium(IV) atom adopts the same coordination geometry as that in **1**. The selenite group is tetradentate and bridges four copper(II) ions. The O11 and O13 atoms are unidentate whereas O12 is bidentate. The interconnection of copper(II) centers by bridging selenite groups resulted in (001) and (002) layers. Two-membered Cu_2O_2 rings and four-membered Cu-(O-Se-O)$_2$-Cu rings are evident in the 2D layer. The Cu···Cu separations within a Cu_2O_2 two-membered ring is 3.183(1) Å, whereas those within four-membered rings are

Table 2. Selected bond lengths [Å] and angles [°] for compounds **1–6**.[a]

	$[H_2pip][Cu(SeO_3)_2]$ (**1**)		
Cu1−O3#1	1.965(6)	Cu1−O3	1.965(6)
Cu1−O2#2	1.982(7)	Cu1−O2#3	1.982(7)
hydrogen bonds:			
N1···O1	2.70(1)	N1−H01b···O1	172.8
	$Cu(C_3H_4N_2)(SeO_3)$ (**2**)		
Cu1−O13#1	1.930(7)	Cu1−O12#2	1.959(7)
Cu1−N1	2.005(8)	Cu1−O11	2.080(7)
Cu1−O12#3	2.237(7)		
$[H_2en][Cu(HSeO_3)_2Cl_2]$ (**3**)			
Cu1−O3#1	1.966(7)	Cu1−O3#2	1.966(7)
Cu1−O1	1.974(7)	Cu1−O1#3	1.974(7)
Cu1−Cl1#3	2.765(3)	Cu1−Cl1	2.765(3)
Se1−O1	1.687(7)	Se1−O3	1.692(7)
Se1−O2	1.758(7)		
hydrogen bonds:			
N1···O2	2.861(12)	N1···O1#1	2.997(12)
	$[H_2en][Co(HSeO_3)_2Cl_2]$ (**4**)		
Co1−O1	2.078(2)	Co1−O1#1	2.078(2)
Co1−O3#2	2.079(2)	Co1−O3#3	2.079(2)
Co1−Cl1	2.533(8)	Co1−Cl1#1	2.533(8)
Se1−O1	1.680(2)	Se1−O3	1.684(2)
Se1−O2	1.753(2)		
hydrogen bonds:			
N1···O2	2.854(3)	N1···O1#3	2.869(4)
	$[H_2en][Cu_2(SeO_3)_2(HSeO_3)]_2{\cdot}H_2O$ (**5**)		
Cu1−O3#1	1.931(7)	Cu1−O4	1.972(7)
Cu1−O1	1.980(7)	Cu1−O7	1.986(8)
Cu1−O4#2	2.450(8)	Cu2−O5#3	1.947(8)
Cu2−O9#4	1.954(8)	Cu2−O2#5	1.977(7)
Cu2−O6	1.978(7)	Cu2−O2	2.386(7)
hydrogen bonds:			
N1···O1w	2.97(2)	N1···O8#6	3.00(2)
N1−H01a···O1w	134.2	N1−H01c···O8#6	123.5
	$[H_2pip][Cu_2(Se_2O_5)_3]$ (**6**)		
Cu1−O11	1.972(4)	Cu1−O2	1.975(4)
Cu1−O14#1	1.975(4)	Cu1−O4	1.988(4)
Cu1−O7	2.429(4)	Cu1−O12#2	2.498(4)
Cu2−O5#3	1.940(4)	Cu2−O8#4	1.958(4)
Cu2−O10	1.985(4)	Cu2−O3#5	1.993(4)
Cu2−O15	2.427(4)	Cu2−O9#6	2.519(4)

[a] Symmetry transformations used to generate equivalent atoms: For **1**: #1 $-x+1, -y+1, -z+1$; #2 $x-1, y, z$; #3 $-x+2, -y+1, -z+1$; for **2**: #1 $-x, -y+1, -z+1$; #2 $x+1/2, -y+1/2, -z+1$; #3 $-x+1/2, y+1/2, z$; for **3**: #1 $-x, y-1/2, -z+1/2$; #2 $x, -y+3/2, z+1/2$; #3 $-x, -y+1, -z+1$; for **4**: #1 $-x, -y+1, -z+1$; #2 $x, -y+3/2, z+1/2$; #3 $-x, y-1/2, -z+1/2$; for **5**: #1 $-x+1, -y, -z$; #2 $-x, -y, -z$; #3 $-x, -y, -z+1$; #4 $-x, -y+1, -z$; #5 $-x+1, -y, -z+1$; #6 $x+1, y-1, z+1$; #7 $-x+1, -y-1, -z+1$; #8 $-x, -y-1, -z+1$; #9 $x, y-1, z+1$; for **6** #1 $x, y-1, z$; #2 $-x+3/2, y-1/2, -z+1/2$; #3 $x-1/2, -y+1/2, z-1/2$; #4 $x, y+1, z$; #5 $x-1/2, -y+3/2, z-1/2$; #6 $-x+1/2, y+1/2, -z+1/2$.

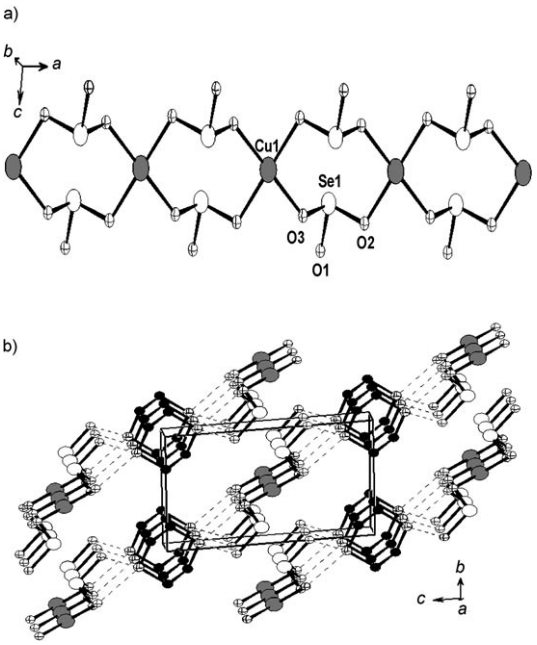

Figure 2. a) 1D Copper(II) selenite chain in **1**; b) view of the structure of **1** down the *a* axis. Cu, Se, O, C and N are drawn as medium gray, white, crossed, black and octand circles, respectively. Hydrogen bonds are drawn as dotted lines.

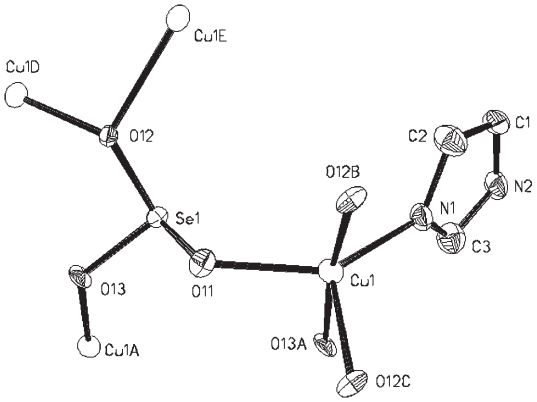

Figure 3. ORTEP representation of the selected unit in **2**. The thermal ellipsoids are drawn at 50% probability. Symmetry codes for generated atoms: a) -x, $-y+1, -z+1$; b) $x+1/2, -y+1/2, -z+1$; c) $-x+1/2, y+1/2, z$; d) $x-1/2, -y+1/2, -z+1$; e) $-x+1/2, y-1/2, z$.

4.805(1) and 5.252(1) Å, respectively. The interlayer distance is ≈8.3 Å. The unidentate imidazole ligands project between the layers and serve to cross-link adjacent inorganic layers through weak π···π interactions (Figure 4). The distance between two parallel $C_3H_4N_2$ rings from two neighboring inorganic layers is ≈3.794 Å.

$[H_2en][M(HSeO_3)_2Cl_2]$ (en = ethylenediamine; M = Cu 3, Co 4): Compounds **3** and **4** are isostructural with the compound $[H_2en][CdCl_2(HSeO_3)_2]$,[16] thus the discussion will be limited to details that are relevant to magnetic studies. The metal centers in **3** or **4** are in an octahedral environment consisting of four O atoms from $HSeO_3$ groups and two Cl^- ligands (Figure 5). The octahedra exhibit a Jahn–Teller distortion as evidence by the axial Cu–Cl distances of 2.765(3) Å which are much longer than the four basal Cu–O distances [1.966(7)–74(7) Å] (Table 2). The connection of copper(II) ions in **3** by bidentate bridging hydrogen selenite groups leads to (100) inorganic layers based on $Cu_4Se_4O_8$ eight-membered rings (Figure 6a). Each copper(II) ion is bridged to four other Cu ions through hydrogen selenite groups with a Cu···Cu separation of 5.906 Å. The corresponding Co···Co separation in **4** is 6.082 Å. The O2 is pro-

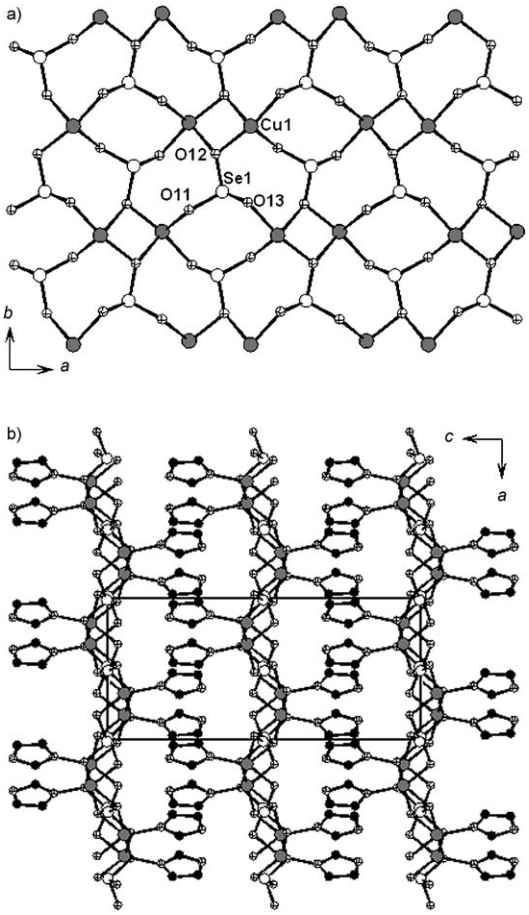

Figure 4. a) 2D Copper(II) selenite layer in **2**; b) view of the structure of **2** down the *b* axis. Cu, Se, O, C and N are drawn as medium gray, white, crossed, black and octand circles, respectively.

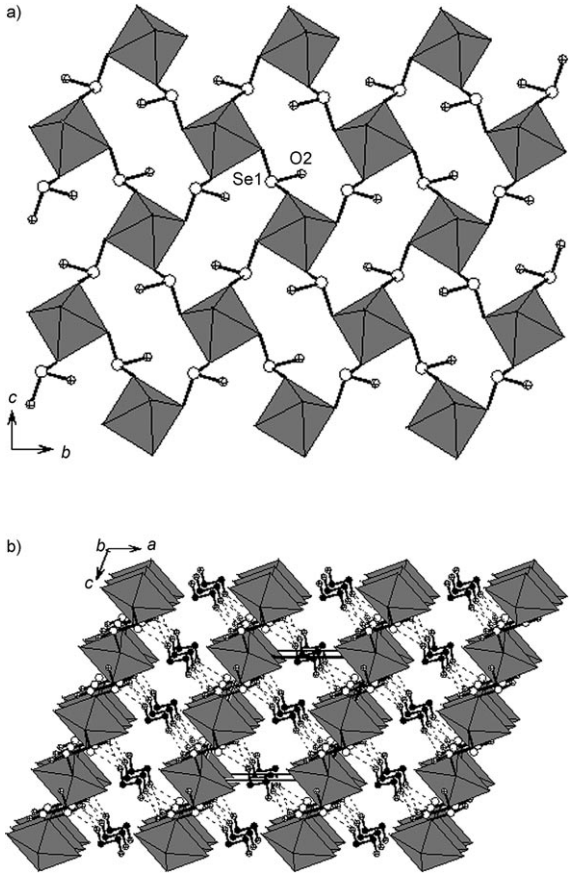

Figure 6. a) 2D Copper(II) hydrogen selenite layer in **3**; b) view of **3** down the *b* axis. CuO_4Cl_2 octahedra are shaded in medium gray. Se, O, C and N are drawn as white, crossed, black and octand circles, respectively. Hydrogen bonds are drawn as dotted lines.

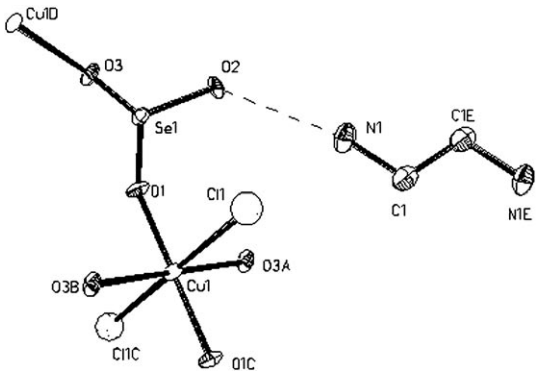

Figure 5. ORTEP representation of the selected unit in **3**. The thermal ellipsoids are drawn at 50% probability. Symmetry codes for generated atoms: a) $-x$, $y-1/2$, $-z+1/2$; b) x, $-y+3/2$, $z+1/2$; c) $-x$, $-y+1$, $-z+1$; d) $-x$, $y+1/2$, $-z+1/2$; e) $-x+1$, $-y$, $-z+1$.

tonated and is therefore not involved in metal coordination. The interlayer distances are 9.0 and 8.7 Å, respectively for compounds **3** and **4**. The doubly protonated template cations are located between the interlayer spaces and are hydrogen bonded to the uncoordinated O atoms of the hydrogen selenite groups (O2 (Table 2, Figure 6b).

$[H_2en][Cu_2(SeO_3)_2(HSeO_3)]_2 \cdot H_2O$ (5): When CuCN is used as the Cu source instead of $CuCl_2 \cdot 2H_2O$ in the preparation of **3**, the new selenite–hydrogen selenite compound **5** with a pillared layered structure is isolated. The asymmetric unit of **5** consists of seventeen independent non-hydrogen atoms, fourteen of which belong to the anionic framework (2 Cu, 3 Se and 9 O) and two of which are from the ethylenediamine (one N atom and one C atom) (Figure 7). An interstitial water molecule was modeled at 50% occupancy. Both Cu1 and Cu2 are five coordinate with a distorted "4+1" square-pyramidal geometry. The axial Cu-O bond lengths (2.450(7) Å for Cu1 and 2.386(7) Å for Cu2) are significantly longer than the remaining Cu–O distances [1.931(7)–1.986(8) Å] (Table 2). Both $Se1O_3$ and $Se2O_3$ groups are tetradentate metal linkers, two O atoms of the selenite groups are unidentate and the third one is bidentate. The $HSe3O_3$ group is disordered and bidentate with the O8 atom being uncoordinated. Based on the Se–O distances, its coordination mode as well as the requirement for charge balance, this group is assigned as a hydrogen selenite group.

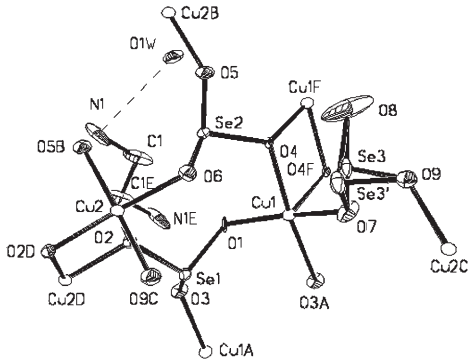

Figure 7. ORTEP representation of a selected unit in compound **5**. The thermal ellipsoids are drawn at 50% probability. Symmetry codes for generated atoms: a) $-x+1, -y, -z$; b) $-x, -y, -z+1$; c) $-x, -y+1, -z$; d) $-x+1, -y, -z+1$; e) $-x+1, -y-1, -z+1$; f) $-x, -y, -z$.

The connection of copper(II) ions by the bridging $Se1O_3$ and $Se2O_3$ groups results in a (020) copper(II) selenite layer (Figure 8a). The layer is based on Cu_2O_2 dimeric units with intra-cluster Cu···Cu separations of 3.275 and 3.409 Å, respectively. The Cu···Cu separations within the Cu-(O-Se-O)$_2$-Cu rings are 4.665(2), 4.801(2) and 5.241(2) Å, respectively. The copper(II) selenite layers are further cross-linked by $HSe3O_3$ groups into a pillared layered architecture (Figure 8b). The closest interlayer Cu···Cu separation is 5.575(2) Å. Two types of tunnels along *a* axis are evident (Figure 7b), the first being a long narrow channel with the lone pairs oriented toward the interior. The second channel is more open and accommodates the template cations as well as interstitial water molecules. It should be noted that O1w is only 2.57(2) Å away from Cu2 (symmetry code: $-x, -y, 1-z$), which can also be considered as a very weak Cu–O bond. The template cation forms hydrogen bonds with the water molecules as well with the uncoordinated O atom of the hydrogen selenite group (Table 2).

$[H_2pip][Cu_2(Se_2O_5)_3]$ (6): Compound **6** is the first example of an organically templated metal diselenite. To date only three metal hydrogen selenite-diselenites, namely, $[NH_2(CH_2)_4NH_2]_{0.5}[M(HSeO_3)(Se_2O_5)]$ (M = Zn, Co, Ni) have been reported.[15] Compound **6** features a novel 3D architecture with tunnels along the *b* axis. The asymmetric unit of compound **6** consists of 29 independent non-hydrogen atoms, 23 of which belong to the anionic framework (two Cu atoms and three diselenite anions), and six of which are from to the piperazine group (Figure 9). The coordination geometries around both Cu1 and Cu2 atoms can be described as "4+2" Jahn–Teller distorted octahedra. The axial Cu–O bond lengths (Cu1–O7 2.429(4) Å, Cu1–O12g 2.498(4) Å, Cu2–O15 2.427(4) Å and Cu2–O9h 2.519(4) Å) are significantly longer than the basal Cu–O bonds [1.940(4)–1.993(4) Å] (Table 2). The diselenite group containing Se1 and Se2 is tetradentate, and it forms a three-membered chelating ring with Cu1 (O2 and O4) as well as a bridge to two other Cu2 atoms. The other two diselenite anions are also tetradentate metal linkers but no chelate ring is formed. The oxygen atoms bridging two Se atoms (O1, O6 and O13) are not involved in metal coordination.

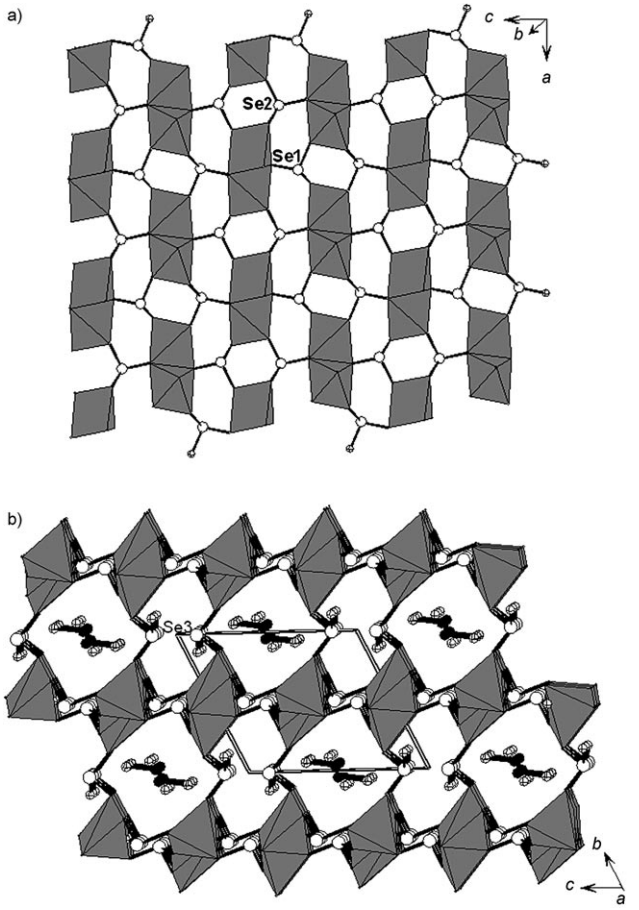

Figure 8. a) (020) 2D Copper(II) selenite layer in **5**; b) view of the structure of **5** down the *a* axis. CuO_5 polyhedra are shaded in medium gray. Se, C, O and N are drawn as white, black, crossed and octand circles, respectively. Hydrogen bonds are drawn as dotted lines.

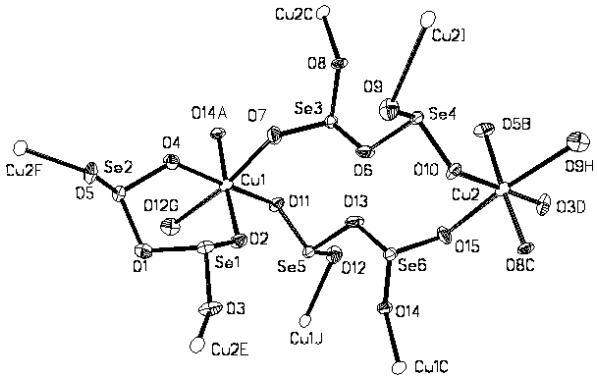

Figure 9. ORTEP representation of a selected unit in **6**. The thermal ellipsoids are drawn at 50% probability. Symmetry codes for generated atoms: a) $x, y-1, z$; b) $x-1/2, -y+1/2, z-1/2$; c) $x, y+1, z$; d) $x-1/2, -y+3/2, z-1/2$; e) $x+1/2, -y+3/2, z+1/2$; f) $x+1/2, -y+1/2, z+1/2$; g) $3/2-x, y-1/2, 1/2-z$; h) $1/2-x, 1/2+y, 1/2-z$; i) $1/2-x, -1/2+y, 1/2-z$; j) $3/2-x, 1/2+y, 1/2-z$. Only one orientation for Se1 and Se2 is shown and the template cation is omitted for the sake of clarity.

The connection of the copper(II) ions by bridging diselenite anions results in a 3D network with large tunnels running along *b* axis (Figure 10). The tunnel is formed by ten-membered rings consisting of four Cu and six Se. The size of the tunnel is estimated to be 11.9×7.4 Å^2 based on the structural data. The doubly protonated piperazine cations are located above the channels.

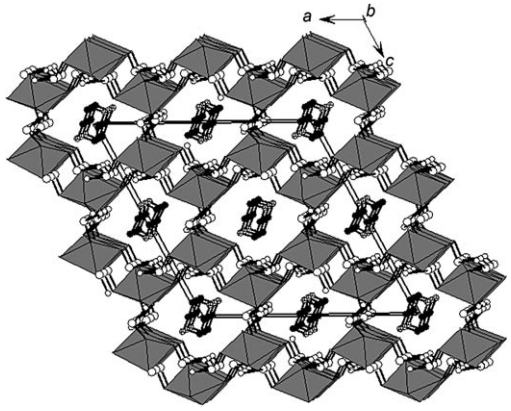

Figure 10. View of the structure of **6** down the *b* axis. CuO_6 octahedra are shaded in medium gray. Se, O, C, and N are drawn as white, crossed, black and octand circles, respectively.

Thermal stability studies

TGA curves for compounds **1–6** indicate that they are stable up to 198 (**1**), 220 (**2**), 177 (**3**) 194 (**4**) 228 (**5**) and 236 °C (**6**) (Figure 11). Upon further increasing the temperature, the water molecule (for **5**), the template molecules and chloride anions (for **3** and **4**) are lost. The loss of the water molecule at 228 °C in **5** can be attributed to its weak coordination to Cu2. The intermediates formed at ≈400 °C are $CoSeO_3$ for compound **4** and $CuSeO_3$ for the five other compounds which undergo further decomposition at higher temperatures with the liberation of SeO_2. The final products are CoO for **4** and CuO for the other compounds.

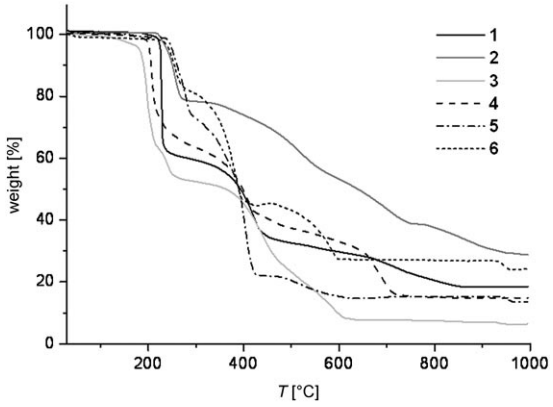

Figure 11. TGA curves for compounds **1–6**.

Magnetic studies

The dc magnetic properties for the new compounds were measured in the temperature range of 2–300 K at the applied magnetic field of 1000 Oe.

$[H_2pip][Cu(SeO_3)_2]$ (1) and $Cu(C_3H_4N_2)(SeO_3)$ (2): The χT and χ versus T plots for $[H_2pip][Cu(SeO_3)_2]$ (**1**) are shown in Figure 12. The value of χ_m is 0.0011 emu mol^{-1} at room temperature and increases smoothly to a maximum of 0.0020 emu mol^{-1} at 85 K, then decreases to a minimum of 0.0016 emu mol^{-1} at 10 K and finally increases to 0.0018 emu mol^{-1} at 2 K. The value of χT at 300 K is 0.35 emu mol^{-1} K, which is close to the expected value for a spin-only case ($\chi_{Cu}T = 0.374$ emu mol^{-1} K, $S = {}^1/_2$). The decrease of χT with upon cooling indicates the presence of antiferromagnetic interaction between copper(II) centers. The magnetic data was fitted by the simple 1D chain model[19] (the Hamiltonian is written as $H = -2J_iJ_{i-1}$). This model produced a good fit to the experimental data over the whole temperature range. The parameters of the fitting are listed in the Table 3.

Table 3. Fitting parameters of magnetic susceptibility for compounds **1–6**.

Compound	Fitting model	J [cm^{-1}]	g	Impurity [%]
1	1D chain	−45	2.2	0.3
2	1D chain	−27	2.23	–
3	square lattice	−34 (−39)[a]	2.17	–
4	square lattice	−4.5 (−4.8)[a]	2.7	–
5	square lattice	−45	2.35	1.5
6	square lattice	−33	2.35	0.7

[a] Obtained from phase diagram.

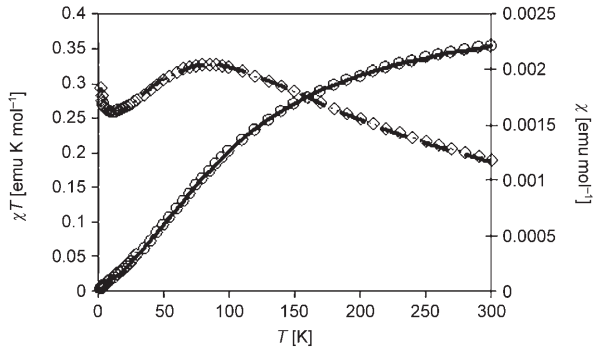

Figure 12. Temperature dependence of the χT product (○) and χ (◇) for **1**. The solid and dashed lines correspond to the best fit to an $S = {}^1/_2$ chain model.

The χT and χ versus T plots for $[Cu(C_3H_4N_2)(SeO_3)]$ (**2**), are similar to those of compound **1** (Figure S1). The plot of χ_m versus T shows a value of 0.0013 emu mol^{-1} at room temperature which increases smoothly to a maximum of 0.0035 emu mol^{-1} at 50 K, then decreases and reaches a minimum of 0.002105 emu mol^{-1} at 4 K and finally increases to

0.002146 emu mol^{-1} at 2 K. The value of χT at 300 K is 0.39 emu mol^{-1} K, which is very close to the expected value for a spin-only case ($\chi_{Cu}T = 0.374$ emu mol^{-1} K, $S = 1/2$). The decrease in χT from room temperature indicates an antiferromagnetic interaction between copper(II) centers. The parameters of the magnetic fitting are listed in the Table 3.

$[H_2en][Cu(HSeO_3)_2Cl_2]$ (3): The χT and χ versus T plots for **3** are shown in Figure S2, Supporting Information. The value of χT at 300 K is 0.38 emu mol^{-1} K, which is close to the expected value for a spin-only case ($\chi_{Cu}T = 0.374$ emu mol^{-1} K, $S = 1/2$). The plot of χ versus T shows a value of 0.0012 emu mol^{-1} at room temperature which increases smoothly to 0.0032 emu mol^{-1} at $\approx$45 K, then reaches a minimum of 0.0030 emu mol^{-1} K at $\approx$24 K and finally increases again at lower temperatures and reaches a value of 0.054 emu mol^{-1} K at 2 K. The χT versus T plot reveals a decrease in χT with cooling which reaches a minimum of 0.068 emu mol^{-1} K at 20 K, after which temperature it increases abruptly and reaches a maximum at 10 K ($\chi T_{max} =$ 0.54 emu mol^{-1} K) and finally decreases again at lower temperatures. These data are in accord with a ferromagnetic interaction between copper(II) ions below 20 K. The magnetic analysis was carried out by using the square lattice model.[20] The parameters of the fitting are listed in the Table 3.

$[H_2en][Co(HSeO_3)_2Cl_2]$ (4): The χT and χ versus T plots for **4** are shown in Figure 13. The value of χT at 300 K is 3.04 emu mol^{-1} K, which is much higher than the expected value for a spin-only case ($\chi_S T = 1.875$ emu mol^{-1} K, $S = 3/2$), as expected for an orbital contribution. As the temperature is lowered, the χT value decreases and reaches a minimum of 1.35 emu mol^{-1} K at 16 K. Below 16 K, χT increases abruptly and reaches a maximum at $\approx$7.5 K ($\chi T_{max} =$ 8.8 emu mol^{-1} K) and finally decreases again at lower temperatures. The plot of χ versus T shows a value of 0.01 emu mol^{-1} at room temperature, which increases smoothly to 0.045 emu mol^{-1} at 26 K, then finally decreases again at lower temperatures reaches to 6.17×10^{-5} emu mol^{-1} K at 2 K. The parameters of the fitting of the magnetic data according to the square lattice model are listed in the Table 3.

The more accurate fit can be obtained assuming that the $^4T_{1g}$ ground state for high-spin octahedral cobalt(II) is subject of unquenched spin-orbit coupling as well as zero-field splitting effects.[21] Unfortunately, there is no expression that simultaneously accounts for both factors. The Hamiltonian for spin-orbit coupling is written as: $H = -\lambda LS$. The χT expression for a mononuclear cobalt(II) complex in an octahedral environment is provided in Equation (1).[21]

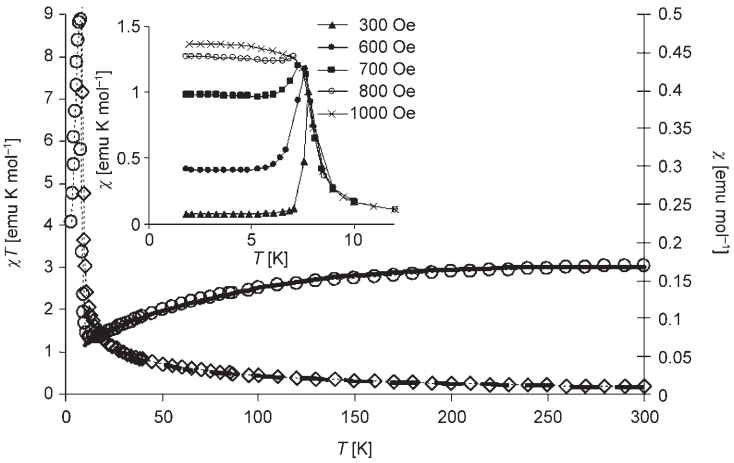

Figure 13. Temperature dependence of the χT product (○) and χ (◇) for **4**. The solid and dashed lines correspond to the best fit to the spin-orbit coupling model. Inset: Temperature dependence of the χ at different applied magnetic fields.

In this equation, $x = \lambda/k_B T$, (λ is the spin-orbit coupling parameter which is -170 cm^{-1} for the free ion) and A is a measure of the crystal field strength due to the interelectronic repulsions (1.5 for a weak field, 1.0 for a strong field and 1.32 for a free ion). Due to the magnetic interactions between ions, the expression in Equation (1) was corrected using the molecular field approximation [Eq. (2)] where χ is the experimental exchange-coupled magnetic susceptibility, χ_{Co} is the magnetic susceptibility in the absence of the exchange field, zJ is the exchange parameter; the other symbols have their usual meanings.[22]

$$\chi = \frac{3\chi_{Co}}{1-(zJ/Ng^2\beta^2)\chi_{Co}} \qquad (2)$$

The magnetic data were fitted to Equation (2) in the temperature range of 2–300 K with parameters $\lambda = -140$ cm^{-1}, and $A = -1.3$ and shown in Figure 14. Taking into account that $\lambda = k\lambda_{free\,ion}$, where k is a reduction of the spin-orbit coupling due to covalency, k is 0.7. The value of $zJ = -3.0$ cm^{-1} indicates that there is antiferromagnetic exchange between cobalt(II) ions.

$[H_2en][Cu_2(SeO_3)_2(HSeO_3)]_2 \cdot H_2O$ (5): The χT and χ versus T plots for **5** are shown in Figure 15. The value of χT at 300 K is 0.71 emu mol^{-1} K, which is close to the expected value for two magnetically isolated $S = 1/2$ copper(II) ions. Upon cooling, the χT value decreases continuously to 0.007 emu mol^{-1} K at 2 K. The plot of χ versus T shows a value of 0.0024 emu mol^{-1} at room temperature, which in-

$$\chi_{Co}T = \frac{\frac{7(3-A)^2x}{5}+\frac{12(2+A)^2}{25A}+\left[\frac{2(11-2A)^2x}{45}+\frac{176(2+A)^2}{675A}\right]x\exp\left(\frac{-5Ax}{2}\right)+\left[\frac{(5+A)^2x}{9}-\frac{20(2+A)^2}{27A}\right]\exp(-4Ax)}{\frac{8x}{3}\left[3+2\exp\left(\frac{-5Ax}{2}\right)+\exp(-4Ax)\right]} \qquad (1)$$

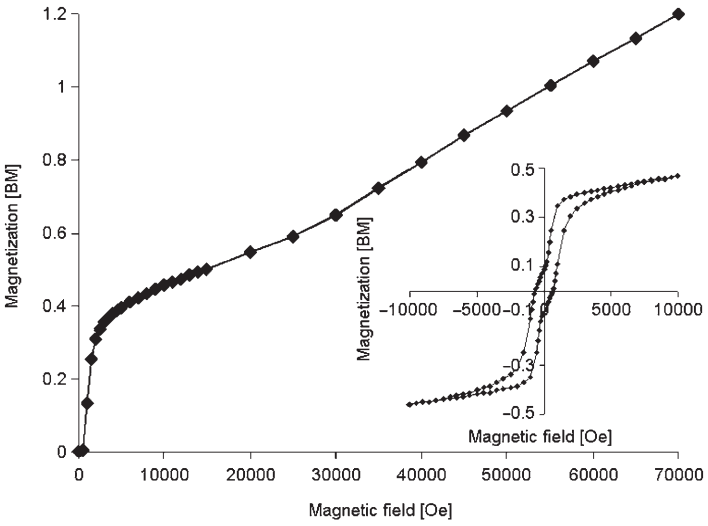

Figure 14. Field dependent magnetization and hysteresis loops (insets) for compounds **4** measured at 1.8 K.

creases smoothly to 0.0037 emu mol^{-1} at 100 K, then reaches a minimum of 0.00075 emu mol^{-1} K at 17 K and finally increases again at lower temperatures. The parameters of the fitting of the magnetic data according to the square lattice model are listed in the Table 3.

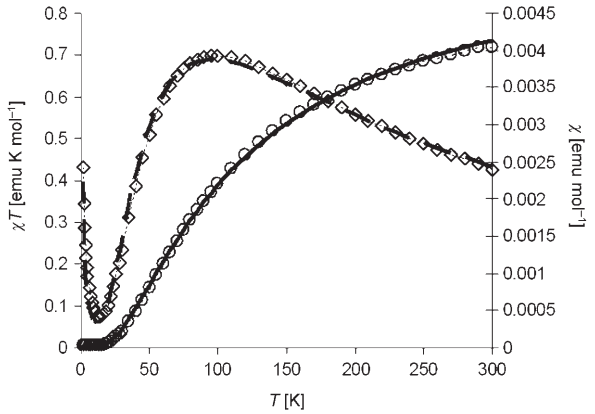

Figure 15. Temperature dependence of the χT product (○) and χ (◇) for **5**. The solid and dashed lines correspond to the best fit to the square lattice model.

$[H_2pip][Cu_2(Se_2O_5)_3]$ (6): The χT and χ versus T plots for $[H_2pip][Cu_2(Se_2O_5)_3]$ (**6**) are shown in Figure S3, Supporting Information. The value of χT at 300 K is 0.87 emu mol^{-1} K, which is close to the expected value for two magnetically isolated $S = {}^1/_2$ copper(II) ions. Upon cooling, the χT value decreases continuously to 0.011 emu mol^{-1} K at 2 K. The plot of χ versus T shows a value of 0.0029 emu mol^{-1} at room temperature, which increases smoothly to 0.0083 emu mol^{-1} at 50 K, then reaches a minimum of 0.0015 emu mol^{-1} K at 10 K and finally increases again at lower temperatures. The parameters of the fitting of the magnetic data according to the square lattice model are listed in the Table 3.

Investigation of spin-flop behavior

Compounds **3** and **4**, which show the most interesting magnetic properties, were subject of more detailed magnetic studies. The application of different magnetic fields in the range of 100–1000 Oe confirmed a sharp maximum in χ at 12 and 8 K for compounds **3** and **4**, respectively, with χ_{max} moving slightly to lower temperatures with a minimal increase in value (Figure S4, Supporting Information and 13 inset). The shape of the sharp maxima in χ is indicative of long-range antiferromagnetic ordering. Application of a field higher than 1 kOe showed no maximum but saturation in χ below T_c. This field-dependent behavior is indicative of a metamagnetic or spin-flop phase transition exhibited for weakly coupled antiferromagnets.[23,24] Evidence for the phase transition was confirmed by ac susceptibility and field-cooled (FC)/zero-field-cooled (ZFC) measurements.

Results of the field-cooled (FC) and zero-field-cooled (ZFC) measurements at 10 Oe exhibit a maximum at $T_c = 12$ and 8 K for compounds **3** and **4**, respectively (Figure S5). Above T_c the magnetization is reversible and behaves similarly for both FC and ZFC. Below T_c, however, there is nonreversibility and bifurcation, consistent with a spontaneous magnetization below a ferromagnetic phase transition. The divergence of dc χ_{ZFC} and χ_{FC} reveals a history dependence of the magnetization process.[25,26]

The zero-field ac susceptibility measurements performed in the range of frequencies from 1 Hz–1 kHz at $H_{ac} =$ 3 Oe kHz indicate that χ' displays a sharp maximum at T_c (Figure S6, Supporting Information). No frequency dependence was observed which excludes glassy behavior.[27]

The magnetic susceptibility (ZFC and real part χ') is known to vary below T_c according to the following expression:[28–30]

$$\chi = \chi_0 \left(1 - \frac{T}{T_c}\right)^{-\gamma} \qquad (3)$$

where γ is the critical exponent and χ_0 is the critical amplitude below T_c. The value of χ, the so-called critical exponent, provides information about the dimensionality and the symmetry of the magnetic lattice undergoing the ordering transition.[28–33] The double logarithmic plots of the χ_{ZFC} and χ' as a function of the reduced temperature are shown in Figure S7, Supporting Information. A fitting of the data to the power law [Eq. (3)] yielded $T_c = 12.1$ K, $\gamma_{AC} = 0.35$, $\gamma_{ZFC} = 0.33$ for compound **3** and $T_c = 7.8$ K, $\gamma_{AC} = 0.66$, $\gamma_{ZFC} = 0.63$ for compound **4**, respectively. The obtained critical exponents are smaller than the values experimentally found in 3D ferromagnets[28] ($\gamma \approx 1.3$) or predicted by mean field theory[31] ($\gamma = 1$). However, they are close to the values found for random anisotropy magnets[29] ($\gamma \approx 0.67$), disordered systems[30] ($\gamma \approx 0.25$–0.5), spin-flop transitions[32] ($\gamma \approx 0.56$) and canted systems[33] ($\gamma \approx 0.35$–0.7).

The magnetization below T_c increases very slowly with increasing field due to strong antiferromagnetic interactions followed by a sharp increase (Figures S8, Supporting Information and 14). The magnetization then increases gradually to 70 kOe without saturation and exhibits a value that is far from the theoretical one expected for copper(II) ($M_s \approx$ 1.1 BM) and Co^{2+} ($Ms \approx 2.3$ BM).[27] Clearly, a higher field is required to reach saturation to a ferromagnetic phase. Assuming the linear increase of the magnetization the expected saturation magnetic fields (H_C) are 2300 kOe and 135 kOe for the compounds **3** and **4**, respectively.

Hysteresis loops measured at 1.8 K are consistent with a weak ferromagnet for both compounds **3** and **4** with coercive fields of 150 and 600 Oe, and remnant magnetization values (M_r) of 0.0007 and 0.09 BM, respectively (Figure S8, Supporting Information and 15, inset). The spontaneous magnetization is therefore due to a spin-canting. The estimated canting angles are 0.04 and 2.2° for compounds **3** and **4**, respectively. This angle is calculated according to the equation $\psi = \tan^{-1}(M_r/M_s)$, where M_r is the remnant magnetization and $M_s = gS$ is the expected saturation magnetization if all the moments are aligned ferromagnetically.[24,34]

The field dependence of the magnetization at different temperatures below T_c have a pronounced sigmoidal shape for both compounds **3** and **4** (Figure S9, Supporting Information and 16). The calculated derivatives dM/dH also show the obvious transitions (Figure S9, Supporting Information and 16, inset) around 800 ± 100 Oe, although the exact value for the peaks decrease with temperature. The behavior is due to a spin-flop transition, which occurs if Ising-like anisotropy is small compared with the weak antiferromagnetic interaction.[29,35] In this case the antiparallel spin alignment changes to a perpendicular orientation to the applied magnetic field.[26] To obtain a more accurate estimate of the transition field, AC susceptibility measurements as a function of the applied DC magnetic field were performed (Figure S10, Supporting Information and 17)[26,36] using a 10 Hz oscillating AC field of 3 Oe. The peaks around the spin-flop transition were reproduced with no frequency dependence being observed.

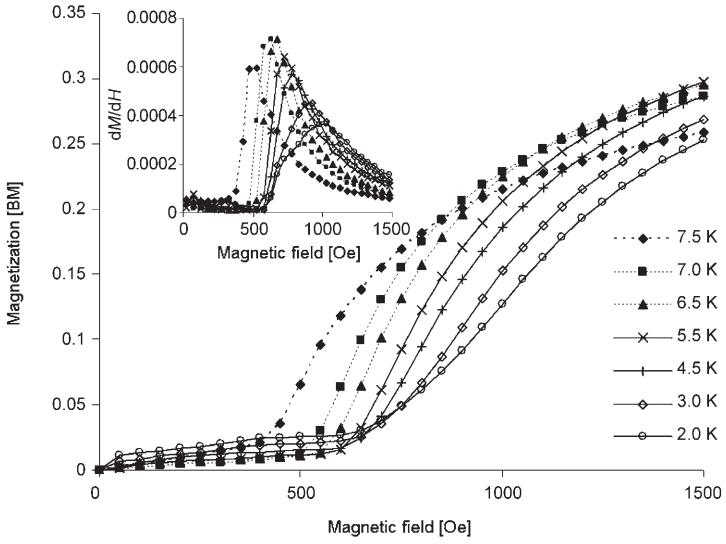

Figure 16. Field dependent magnetization curves and plots of dM/dH vs H (insets) at different temperatures for compounds b.

According to the aforementioned observations, phase diagrams of compounds **3** and **4** were constructed (Figure S11, Supporting Information and 18). The weak ferromagnet-spin-flop (WFM-SF) boundary experimental points (diamonds) was obtained from the peaks in dM/dH and χ' versus H curves, while the weak ferromagnet/parmagnet WFM-PM boundary (cubes) was obtained from the peaks of $\chi(T)$. The phase transition from the spin-flop state to a field induced ferromagnetic state is not complete at the fields that we were able to apply; clearly a higher field is necessary. These types of phase diagrams are very similar to those reported for a field-induced spin-flop transition, which is common for antifferomagnetic systems with weak anisotropy.[26,36–38]

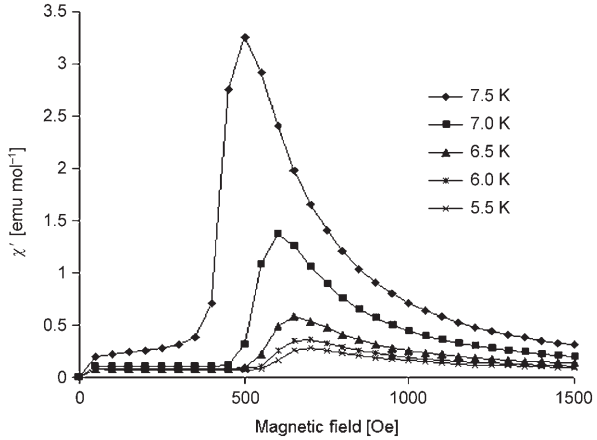

Figure 17. Field dependence of the in-phase contribution to the AC susceptibility signal at different temperatures for compound **4**.

The temperature dependence of the spin-flop field can be linearly extrapolated to $T = 0$ K to obtain $H_{SF}(0) = 0.9$ kOe and 1 kOe for compounds **3** and **4**, respectively. Using mean-field relation:[26,38,39]

$$H_{SF}(0) = [2H_E H_A - H_A^2]^{1/2} \quad (4)$$

$$H_C(0) = 2H_E - H_A \quad (5)$$

H_E and H_A are the exchange and anisotropy fields and using estimated values of H_C, one obtains $H_A = 0.35$ Oe, $H_E =$ 1150 kOe; and $H_A = 7.4$ Oe, $H_E = 67.5$ kOe for compounds **3** and **4**, respectively. The anisotropy constants $\alpha = H_A/H_E$ are $\approx 3 \times 10^{-7}$ and 10^{-4} for these compounds. The low values of the anisotropy constant ($< 10^{-2}$) are typical for the Heisenberg antiferromagnets showing spin-flop transition.[26,39] The estimated exchange constants[38] $J = g\beta H_E/2zS$ are -39 and

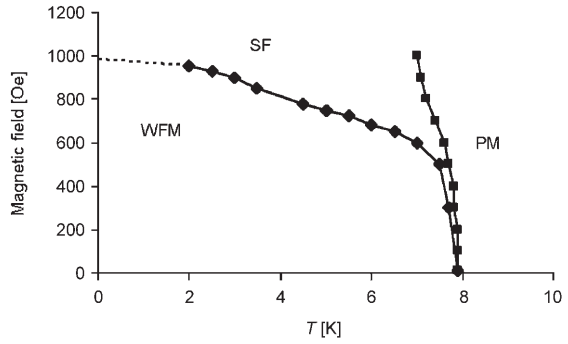

Figure 18. $H(T)$ phase diagram for compound **4**. WFM = weak feromagnetic, SF = spin-flop and PM = paramagnetic states. The diamonds and the cubes represent the experimental data obtained from magnetization $M(H)$ and susceptibility $\chi(T)$ measurements.

$-4.8\,cm^{-1}$ for compounds **3** and **4**, respectively, assuming $z=4$ for quadratic layers and effective spin $S_{eff} = {}^1/_2$ with g effective $g_{eff}=4.3$ for cobalt(II) at low temperature. These parameters are in good agreement with the values obtained from the high temperature susceptibility fit.

Conclusions

In summary, six new copper(II) or cobalt(II) selenites with 1D to 3D structures with organic constituents were prepared by using hydro-/solvothermal methods. It was found that the copper source and the solvent as well as the organic template influence the compositions and structures of the particular metal selenite isolated. Depending on the experimental conditions, the selenium(IV) ions can exist as a selenite anion (SeO_3^{2-}) as in **1** and **2**, a hydrogen selenite anion ($HSeO_3^-$) as in **3** and **4**, or a diselenite anion ($Se_2O_5^{2-}$) as in **6**. It is also possible for the metal selenite compound to have a combination of two different types of selenite anions such as $HSeO_3^-$ and SeO_3^{2-} in **5**, and $HSeO_3^-$ and $Se_2O_5^{2-}$ in $[NH_2(CH_2)_4NH_2]_{0.5}[M(HSeO_3)(Se_2O_5)]$ (M = Zn, Co, Ni).[15] The richness of the structural chemistry of Copper(II) selenites is due to the varied coordination geometries that the copper(II) ion can adopt. All of the compounds exhibit fairly strong antiferromagnetic interactions. Compounds **3** and **4** behave as a weak ferromagnets below the critical temperatures of $T_c = 12$ and 8 K, respectively. The spin-canting angles were estimated to be 0.04 and 2.2°, respectively. Magnetic measurements as a function of the field display the onset of spin-flop phase transitions around 800 ± 100 Oe for both of these compounds.

Experimental Section

Materials and methods: All chemicals were purchased from commercial sources and used without further purification. The Cu, Co, Se and Cl analyses were carried out with an ICPQ-100 spectrometer whereas C, H and N analyses were performed on a German Elementary Vario EL III instrument. IR spectra were recorded on a Magna 750 FT-IR spectrometer photometer as KBr pellets in the range of 4000–400 cm^{-1}. Thermogravimetric analyses were carried out with a NETZSCH STA 449C unit at a heating rate of 10 °C min^{-1} under a nitrogen atmosphere. The XRD powder patterns were collected on a Philips X'Pert-MPD diffractometer using graphite monochromated $Cu_{K\alpha}$ radiation in the angular range $2\theta =$ 5–70° with a step size of 0.02° and a counting time of 3 s per step. Magnetic susceptibility measurements were carried out on a Quantum Design MPMS-XL SQUID magnetometer. The raw data were corrected for the susceptibility of the container and the diamagnetic contributions of the sample using Pascal's constants.

$[H_2pip][Cu(SeO_3)_2]$ (1): A mixture of CuCN (0.049 g, 0.547 mmol), SeO_2 (0.224 g, 2.020 mmol), piperazine (0.083 g, 0.964 mmol), ethanol (5 mL) and H_2O (1 mL) was stirred under ambient conditions until it was homogeneous. The resulting mixture was sealed into an autoclave equipped with a Teflon liner (25 mL) and heated at 100 °C for 4 d. The initial and final pH values of the solution did not show appreciable change and were close to 5.0. Blue brick-shaped crystals of **1** were collected in ca. 68 % yield (based on Cu). IR (KBr): $\tilde{\nu}$ = 3001 m, 2966 w, 1618 s, 1493 s, 1446 m, 1376 s, 1321 s, 1300 s, 1219 m, 1120 w, 1091 s, 1079 s, 1028 s, 983 s, 883 s, 807 m, 732 vs, 616 m, 534 s, 462 s cm^{-1}; elemental analysis calcd (%) for $C_4H_{12}CuN_2O_6Se_2$: Cu 15.67, Se 38.93, C 11.84, H 2.98, N 6.91; found: Cu 15.98, Se 38.02, C 12.02, H 3.10, N 6.75.

$Cu(C_3H_4N_2)(SeO_3)$ (2): A mixture of CuCl (0.037 g, 0.378 mmol), SeO_2 (0.137 g, 1.236 mmol), imidazole (0.122 g, 1.799 mmol), acetonitrile (5 mL) and H_2O (1 mL) was stirred under ambient conditions. The mixture was sealed in an autoclave equipped with a Teflon liner (25 mL) and heated at 85 °C for 5 d. The initial and final pH values of the solution were ≈5.0. Green brick-shaped crystals of **2** were collected in ca. 21 % yield (based on Cu). IR (KBr): $\tilde{\nu}$ = 3141 m, 2961 w, 2865 w, 1547 m, 1498 w, 1442 s, 1329 s, 1258 w, 1180 m, 1109 m, 1091 s, 1070 s, 951 w, 853 s, 832 m, 800 m, 756 s, 738 s, 687 vs, 650 s, 623 m, 527 m, 480 s cm^{-1}; elemental analysis calcd (%) for $C_3H_4CuN_2O_3Se$: Cu 24.57, Se 30.54, C 13.93, H 1.56, N 10.83; found: Cu 24.43, Se 30.96, C 13.98, H 1.68, N 10.26.

$[H_2en][Cu(HSeO_3)_2Cl_2]$ (3): Compound **3** was synthesized by heating a mixture of $CuCl_2{\cdot}2H_2O$ (0.083 g, 0.489 mmol), SeO_2 (0.224 g, 2.020 mmol), ethylenediamine (0.12 mL, 1.800 mmol), acetonitrile (5 mL) and H_2O (1 mL) at 85 °C for 5 d. The pH value of the solution remained at ≈5 during the course of the reaction. Light green platelet crystals of **3** were collected in ca. 57 % yield (based on Cu). IR (KBr): $\tilde{\nu}$ = 3464 w, 3020 br, 2291 w, 1583 s, 1504 s, 1469 m, 1326 s, 1193 s, 1053 s, 1032 s, 1015 w, 830 m, 737 vs, 673 vs, 523 vs, 428 s cm^{-1}; elemental analysis calcd (%) for $C_2H_{12}Cl_2CuN_2O_6Se_2$: Cu 14.04, Se 34.90, Cl 15.67, C 5.31, H 2.67, N 6.19; found: Cu 14.23, Se 34.96, Cl 15.62, C 5.42, H 2.87, N 6.89.

$[H_2en][Co(HSeO_3)_2Cl_2]$ (4): Compound **4** was synthesized by heating a mixture of $CoCl_2{\cdot}6H_2O$ (0.352 g, 1.479 mmol), SeO_2 (0.334 g, 3.015 mmol), ethylenediamine (0.12 mL, 1.800 mmol) dichloromethane (4.8 mL) and H_2O (1 mL) at 100 °C for 4 d. The initial and final pH values were ≈2. Purple brick-shaped crystals of **4** were collected in ca. 71 % yield (based on Co). The addition of dichloromethane reduces the solubility of compound in reaction media and helps its crystallization. IR (KBr): $\tilde{\nu}$ = 3444 w, 3049 br, 2363 m, 1593 s, 1571 w, 1510 s, 1469 m, 1365 w, 1329 m, 1196 s, 1060 s, 1030 m, 1017 w, 832 m, 749 vs, 667 vs, 496 s cm^{-1}; elemental analysis calcd (%) for $C_2H_{12}Cl_2CoN_2O_6Se_2$: Co 13.16, Se 35.26, Cl 15.83, C 5.36, H 2.70, N 6.25; found: Co 13.10, Se 34.97, Cl 15.72, C 5.48, H 2.88, N 6.21.

$[H_2en][Cu_2(SeO_3)_2(HSeO_3)]_2{\cdot}H_2O$ (5): Single crystals of compound **5** were obtained by heating a mixture of CuCN (0.088 g, 0.984 mmol), SeO_2 (0.221 g, 1.991 mmol), ethylenediamine (0.12 mL, 1.800 mmol), acetonitrile (5 mL) and H_2O (1 mL) at 85 °C for 5 days. The initial and final pH values are both close to 5. A single phase of **5** was synthesized by using ethanol (5 mL) instead of acetonitrile (5 mL) and reacted at 100 °C for 5 d. Green powder samples of **5** were collected in ca. 46 % yield (based on Cu). IR (KBr): $\tilde{\nu}$ = 3459 w, 3152 w, 2155 w, 1614 w, 1569 s, 1488 w, 1462 m, 1333 m, 1122 w, 1067 m, 1029 m, 718 vs, 649 s, 532 s, 485 s cm^{-1}; elemental analysis calcd (%) for $CH_7Cu_2NO_{9.50}Se_3$: Cu 23.15, Se 43.14, C 2.19, H 1.29, N 2.55; found: Cu 23.11, Se 43.10, C 2.23, H 3.01, N 2.51.

Table 1. Crystal data and structure refinements for six compounds.

Compound	**1**	**2**	**3**	**4**	**5**	**6**
formula	$C_4H_{12}CuN_2O_6Se_2$	$C_3H_4CuN_2O_3Se$	$C_2H_{12}Cl_2CuN_2O_6Se_2$	$C_2H_{12}Cl_2CoN_2O_6Se_2$	$C_2H_{14}Cu_4N_2O_{19}Se_6$	$C_4H_{12}Cu_2N_2O_{15}Se_6$
F_w	405.62	258.58	452.50	447.89	1098.08	929.00
space group	$P\bar{1}$	*Pbca*	$P2_1/c$	$P2_1/c$	$P\bar{1}$	$P2_1/n$
a [Å]	5.3351(8)	7.5575(6)	9.046(1)	8.692(1)	7.5337(8)	17.0769(19)
b [Å]	6.1263(9)	9.3285(8)	7.1781(8)	7.3569(6)	8.4545(8)	7.1158(7)
c [Å]	8.2960(12)	16.6741(14)	9.3812(11)	9.6872(11)	9.2088(10)	17.478(2)
α [°]	92.070(3)	90	90	90	65.115(2)	90
β [°]	98.573(3)	90	111.048(2)	112.776(4)	88.600(2)	117.360(4)
γ [°]	115.604(3)	90	90	90	72.0560(10)	90
V [Å^3]	240.25(6)	1175.53(17)	568.51(11)	571.17(10)	502.43(9)	1886.2(4)
Z	1	8	2	2	1	4
ρ_{calcd} [g cm^{-3}]	2.804	2.922	2.643	2.604	3.629	3.271
μ [mm^{-1}]	9.860	9.843	8.802	8.352	15.140	13.911
crystal size [mm]	0.10×0.10×0.04	0.08×0.06×0.06	0.14×0.12×0.08	0.16×0.10×0.08	0.10×0.08×0.02	0.15×0.15×0.10
F(000)	195	984	434	430	512	1728
reflns collected	1227	5382	2821	4270	3111	13963
independent reflns 828	1035	1004	1311	1704	4319	
R_{int}	0.0395	0.0909	0.0616	0.0266	0.0431	0.0388
obsd data [$I>2\sigma(I)$]	729	820	833	1211	1364	3734
data/restraints/parameters	828/0/71	1035/0/92	1004/0/71	1311/0/70	1704/0/164	4319/0/269
GOF on F^2	1.212	1.203	1.275	1.141	1.096	1.140
$R1$, $wR2$ ($I>2\,\sigma(I)$)[a]	0.0477, 0.1011	0.0623, 0.1106	0.0602, 0.1187	0.0254, 0.0534	0.0522, 0.1178	0.0401, 0.0762
$R1$, $wR2$ (all data)	0.0590, 0.1091	0.0884, 0.1219	0.0786, 0.1251	0.0294, 0.0553	0.0698, 0.1284	0.0507, 0.0812

[a] $R1=\Sigma||F_o|-|F_c||/\Sigma|F_o|$, $wR2=\{\Sigma w[(F_o^2)^2-(F_c^2]^2/\Sigma w[(F_o^2]^2\}^{1/2}$.

$[H_2pip][Cu_2(Se_2O_5)_3]$ (6): Single crystals of **6** were synthesized by heating a mixture of $CuCl_2{\cdot}2H_2O$ (0.085 g, 0.498 mmol), SeO_2 (0.441 g, 3.980 mmol), piperazine (0.161 g, 1.879 mmol), ethanol (5 mL) and H_2O (1 mL) at 100 °C for 5 d. Light green brick-shaped crystals of **6** were collected in ca. 52% yield (based on Cu). The initial and final pH values were ≈5. IR (KBr): $\tilde{\nu}$ = 3451 br, 2924 m, 2715 w, 2573 w, 2468 m, 1624 s, 1457 w, 1444 m, 1375 w, 1316 w, 1169 w, 1088 s, 1009 m, 969 m, 891 w, 840 m, 760 vs, 588 s, 494 vs cm^{-1}; elemental analysis calcd (%) for $C_4H_{12}Cu_2N_2O_{15}Se_6$: Cu 13.68, Se 51.00, C 5.17, H 1.30, N 3.02; found: Cu 13.56, Se 49.62, C 5.32, H 1.33, N 3.00.

X-ray Crystallography: Single crystals of compounds **1** to **6** were subjected to X-ray studies on a Siemens Smart CCD or Rigaku Mercury CCD diffractometer equipped with graphite-monochromated $Mo_{K\alpha}$ radiation ((λ = 0.71073 Å). Intensity data were collected by the narrow frame method at 293 K and corrected for Lorentz and polarization effects as well as for absorption by the SADABS program or the Multi-Scan technique.[40] All structures were solved by direct methods and refined by full-matrix least-squares cycles in SHELX-97.[40] All non-hydrogen atoms were refined with anisotropic thermal parameters. Hydrogen atoms attached to C and N atoms as well as those of the hydrogen selenite groups were located at geometrically calculated positions and refined with isotropic thermal parameters. The hydrogen positions for water molecules in **5** were not refined. The Se3 atom in compound **5** and the Se1 and Se2 atoms in compound **6** are disordered and each exhibits two orientations (Se3 and Se3′, Se1 and Se1′, Se2 and Se2′). The water molecule, O1w in compound **5** with a short O1w···O1w contact (symmetry code: $-x$, $-y-1$, $-z+1$) of 1.75(4) Å is disordered and its occupancy factor was set to 0.5. Crystallographic data and structural refinement parameters for the six compounds are summarized in Table 1. Important bond distances are listed in Table 2.

CCDC-294545–294550 contain the supplementary crystallographic data for this paper. These data can be obtained free of charge from The Cambridge Crystallographic Data Centre via www.ccdc.cam.ac.uk/data_request/cif.

Acknowledgements

J.G.M. gratefully acknowledges financial support from the National Natural Science Foundation of China (20371047). K.R.D. gratefully acknowledges the Department of Energy (DE-FG03-02ER45999), the National Science Foundation (NIRT-NSF DMR-0103455), the Welch Foundation A1449, and Texas A&M University (TITF) for funding of this research. The SQUID magnetometer was purchased by funds provided by the National Science Foundation (NSF-9974899).

[1] G. Férey, A. K. Cheetham, *Science* **1999**, *283*, 1125–1126.
[2] A. K. Cheetham, G. Férey, T. Loiseau, *Angew. Chem.* **1999**, *111*, 3466–3492; *Angew. Chem. Int. Ed.* **1999**, *38*, 3268–3292.
[3] C. N. R. Rao, S. Natarajan, A. Choudhury, S. Neeraj, A. A. Ayi, *Acc. Chem. Res.* **2001**, *34*, 80–87.
[4] S. Ekambaram, S. C. Sevov, *Inorg. Chem.* **2000**, *39*, 2405–2410.
[5] S. Chakrabarti, S. Natarajan, *J. Chem. Soc. Dalton Trans.* **2002**, 3874–3878.
[6] W. T. A. Harrison, M. L. F. Phillips, A. V. Chavez, T. M. Nenoff, *J. Mater. Chem.* **1999**, *9*, 3087–3092.
[7] B. A. Reisner, A. Tripathi, J. B. Parise, *J. Mater. Chem.* **2001**, *11*, 887–890.
[8] X.-H. Bu, P.-Y. Feng, T. E. Gier, D. Zhao, G. D. Stucky, *J. Am. Chem. Soc.* **1998**, *120*, 13389–13397.
[9] W. T. A. Harrison, M. L. F. Phillips, T. M. Nenoff, E. J. MacLean, S. J. Teat, R. S. Maxwell, *J. Chem. Soc. Dalton Trans.* **2001**, 546–549.
[10] a) H.-S. Ra, K.-M. Ok, P. S. H. Halasyamani, *J. Am. Chem. Soc.* **2003**, *125*, 7764–7765; b) K.-M. Ok, P. S. Halasyamani, *Inorg. Chem.* **2004**, *43*, 4248–4253; c) K.-M. Ok, J. Orzechowski, P. S. Halasyamani, *Inorg. Chem.* **2004**, *43*, 964–968; d) J. Goodey, K.-M. Ok, J. Broussard, C. Hofmann, F. V. Escobedo, P. S. Halasyamani, *J. Solid State Chem.* **2003**, *175*, 3–12.
[11] W. T. A. Harrison, M. L. F. Phillips, J. Stanchfield; T. M. Nenoff, *Angew. Chem.* **2000**, *112*, 3966–3968; *Angew. Chem. Int. Ed.* **2000**, *39*, 3808–3810.
[12] A. Choudhury, D. Udayakumar, C. N. R. Rao, *Angew. Chem.* **2002**, *114*, 166–169; *Angew. Chem. Int. Ed.* **2002**, *41*, 158–161.

[13] a) I. Pasha, A. Choudhury, C. N. R. Rao, *Inorg. Chem.* **2003**, *42*, 409–415; b) H. Nakano, T. Ozeki, A. Yagasaki, *Inorg. Chem.* **2001**, *40*, 1816–1819.
[14] a) Z. Shi, D. Zhang, S.-H. Feng, G.-H. Li, Z.-M. Dai, W.-S. Fu, X.-B. Chen, J. Hua, *J. Chem. Soc. Dalton Trans.* **2002**, 1873–1874; b) Z.-M. Dai, X.-B. Chen, Z. Shi, D. Zhang, G.-H. Li, S.-H. Feng, *Inorg. Chem.* **2003**, *42*, 908–912; c) Z.-M. Dai, Z. Shi, G.-H. Li, D. Zhang, W.-S. Fu, H.-Y. Jin, W. Xu, S.-H. Feng, *Inorg. Chem.* **2003**, *42*, 7396–7402; d) Z.-M. Dai, Z. Shi, G.-H. Li, X.-B. Chen, X.-Y. Lu, Y.-H. Xu, S.-H. Feng, *J. Solid State Chem.* **2003**, *172*, 205–211; e) Z.-M. Dai, G.-H. Li, Z. Shi, W.-S. Fu, W.-J. Dong, J. Xu, S.-H. Feng, *Solid State Sci.* **2004**, *6*, 91–96.
[15] D. Udayakumar, C. N. R. Rao, *J. Mater. Chem.* **2003**, *13*, 1635–1638.
[16] I. Pasha, A. Choudhury, C. N. R. Rao, *Solid State Sci.* **2003**, *5*, 257–262.
[17] F. Millange, C. Serre, T. Cabourdin, J. Marrot, G. Férey, *Solid State Sci.* **2004**, *6*, 229–233.
[18] a) U. Kortz, M. G. Savelieff, F. Y. A. Ghali, L. M. Khalil, S. A. Maalouf, D. I. Sinno, *Angew. Chem.* **2002**, *114*, 4246–4249; *Angew. Chem. Int. Ed.* **2002**, *41*, 4070–4073; b) M.-L. Feng, J.-G. Mao, *Eur. J. Inorg. Chem.* **2004**, 3712–3717.
[19] M. E. Fisher, *Am. J. Phys.* **1964**, *32*, 343–346.
[20] M. E. Lines, *J. Phys. Chem. Solids*, **1970**, *31*, 101–116.
[21] F. E. Mabbs, D. J. Machin, *Magnetism and Transition Metal Complexes*, Chapman and Hall, London, **1973**, pp. 99.
[22] O. Kahn, *Molecular Magnetism*, VCH, New York, **1993**, pp. 26.
[23] D. J. Price, S. R. Batten, B. Moubaraki, K. S. Murray, *Polyhedron* **2003**, *22*, 2161–2167.
[24] A. Marvilliers, S. Parsons, E. Riviere, J.-P. Audiere, M. Kurmoo, T. Mallah, *Eur. J. Inorg. Chem.* **2001**, 1287–1293.
[25] Y. Song, P. Y. Zavalij, N. A. Chernova, M. S. Whittingham, *Chem. Mater.* **2003**, *15*, 4968–4973.
[26] J. L. Manson, C. R. Kmety, F. Palacio, A. J. Epstein, J. S. Miller, *Chem. Mater.* **2001**, *13*, 1068–1073.
[27] L.-M. Zheng, S. Gao, P. Yin, X.-Q. Xin, *Inorg. Chem.* **2004**, *43*, 2151–2156.
[28] a) J. J. Binney, N. J. Dowrick, A. J. Fisher, M. E. J. Newman, *The theory of critical phenomena*, Clarendon, Oxford, **1992**; b) U. Bovensiepen, C. Rudt, P. Poulopoulos, K. Baberscheke, *J. Magn. Magn. Mater.* **2001**, *231*, 65–73.
[29] M. A. Girtu, C. M. Wynn, J. Zhang, J. S. Miller, A. J. Epstein, *Phys. Rev. B* **2000**, *61*, 492–500.
[30] A. Belayachi, J. L. Dormann, M. Nogues, *J. Phys. Condens. Matter* **1998**, *10*, 1599–1619.
[31] H. E. Stanley, *Introduction to phase transitions and critical phenomena*, Clarendon, Oxford, **1971**, p. 308.
[32] H. Kawamura, A. Caille, M. L. Plumer, *Phys. Rev. B* **1990**, *41*, 4416–4421.
[33] J. L. Dormann, A. Belayachi, N. Nogues, *J. Magn. Magn. Mater.* **1992**, *104–107*, 239–240.
[34] F. Palacio, M. Andres, R. Horne, A. J. van Duyneveldt, *J. Magn. Magn. Mater.* **1986**, *54–57*, 1487–1488.
[35] B.-Q. Ma, H.-L. Sun, S. Gao, G. Su, *Chem. Mater.* **2001**, *13*, 1946–1948.
[36] X.-Y. Wang, H.-Y. Wei, Z.-M. Wang, Z.-D. Chen, S. Gao, *Inorg. Chem.* **2005**, *44*, 572–583.
[37] R. L. Carlin, A. J. van Duyneveldt, *Acc. Chem. Res.* **1980**, *13*, 231–236.
[38] L. J. de Jongh, W. D. van Amstel, A. R. Miedema, *Physica* **1972**, *58*, 277–304.
[39] J. L. Manson, Q.-Z. Huang, J. W. Lynn, H.-J. Koo, M.-H. Whagbo, R. Bateman, T. Otsuka, N. Wada, D. N. Argyriou, J. S. Miller, *J. Am. Chem. Soc.* **2001**, *123*, 162–172.
[40] a) G. M. Sheldrick, *Program SADABS*; Universität Göttingen, **1995**; b) CrystalClear ver. 1.3.5. Rigaku Corp., Woodlands, TX, **1999**; c) G. M. Sheldrick, *SHELXTL*, *Crystallographic Software Package*, SHELXTL, Version 5.1, Bruker-AXS, Madison, WI, **1998**.

Received: January 9, 2006
Published online: July 24, 2006

